

Part I

A New Perspective of Shape Recognition to Discover the Phase Transition of Finite-size Clusters

Abstract

An ultrafast shape-recognition technique was used to analyze the phase transition of finite-size clusters, which, according to our research, has not yet been accomplished. The shape of clusters is the unique property that distinguishes clusters from bulk systems, and is comprehensive and natural for structural analysis. In this study, an isothermal molecular dynamics simulation was performed to generate a structural database for shape recognition of Ag-Cu metallic clusters using empirical many-body potential. The probability contour of the shape similarity exhibits the characteristics of both the specific heat and Lindemann index (bond length fluctuation) of clusters. Moreover, our implementation of the substructure to the probability of shapes provides a detailed observation of the atom/shell-resolved analysis, and the behaviors of the clusters were reconstructed based on the statistical information. The method is efficient, flexible, and applicable in any type of finite-size system, including polymers and nanostructures.

Intorduction

Numerous studies have evaluated the thermal properties of a finite-size cluster; the typical method involves isothermally calculating the time or ensemble average of the total energy of a system, constructing a caloric curve, and using the change in temperature demonstrated in the curve to calculate the heat capacity by using either laboratory [1, 2] or computer simulation [3] experiments. The results of numerical simulation experiments are relatively more promising and insightful compared with those of laboratory experiments because they can elucidate atomic or molecular distributions by measuring the bond-length fluctuation and coordination number of trajectory; thus, molecular topologies can be understood by recognizing these measurements as proceeding in one- or two-stage processes [4–8], and determining how they yield cluster-melting scenarios. To evaluate large clusters, scholars have emphasized examining the solidlike-liquidlike structural transformation of pure clusters or the atomic number composition dependence of bimetallic clusters. In particular, the precursors of pure clusters signify that the cluster topology melts as a type of thermodynamic transition [9]. This thermal study involved two strategies for examining cluster topology. First, a common neighbor analysis [10, 11] is used to identify or scrutinize core-shell onion-like geometries [12] and analyze melting as the two-stage process of solidlike-to-liquidlike structural transformation. Second, the curvature distribution of the cluster surface was delineated [13] to determine its relevance to attaining an equilibrium in cluster shape.

To discriminate between geometries, the shape recognition technique has been widely used for virtually screening protein molecule databases in drug design and discovery [14]; however, this strategy is seldom applied to analyze small molecular systems, such as metallic clusters, whose molecular geometries are thermally perturbed. The idea of applying the shape recognition technique to elucidate the structural evolution of cluster melting originated from our observations regarding the fundamental differences in the dynamics of atoms or molecules between finite (e.g., cluster) and bulk infinite systems. A molecule structural database for assessing shape recognition can be generated by performing conventional numerical simulations such as molecular dynamics (MD) and Monte Carlo simulations. To test the generality of the proposed technique, metallic clusters composed of copper and silver atoms of various shapes were used as model systems such as a single icosahedron exhibiting an adatom ($Cu_{13}Ag_1$ and $Ag_{13}Cu_1$), double icosahedron ($Ag_{17}Cu_2$), or systems exhibiting core-shell geometries ($Ag_{32}Cu_6$ and $Ag_{32}Cu_{13}$). The Appendix details the parameterized potential form and the numerical details of the isothermal simulation.

Methods

In this study, an MD trajectory was used to build structural database for analyzing both the statistical and dynamical properties of cluster systems. The ultrafast shape recognition technique developed by Ballester et al. [15] was used to calculate the shape similarity index, ζ , which is defined as follows:

$$\zeta(t) = \left(1 + \frac{1}{16} \sum_{j=1}^{16} |M_{0,j} - M_j(t)|\right)^{-1} \quad (0.1)$$

where $\{M_{0,j}|j = 1, 16\}$ and $\{M_j(t)|j = 1, 16\}$ are the moment descriptors representing the structural signature of the initial configuration at $t = 0$ and that of the configuration at given time t in the trajectory, respectively. To construct these descriptors, first, four strategically distributed reference coordinates were located in the space confining the cluster: the center of mass (COM), the atom closest to the COM, the atom farthest from the COM (FCM), and the atom farthest from the FCM. Second, four sets of atomic distance measurements were computed based on the reference coordinates. Third, the moment analysis method suggested by Cannon et al. [16] was applied, which involved obtaining the mean, variance, skewness, and kurtosis values of each set of atomic distance. Finally, four moments and four reference coordinates yielded 16 moment descriptors ($j = 1, 16$). The shape similarity index was used to measure how the shape of the trajectory deviated from that of the initial configuration. After forming the MD trajectory, specific atoms could be excluded using atomic labeling to calculate the four reference coordinates and four moments such that ζ targeted not only structures containing whole atoms but also cluster substructures. Such manipulation enabled tracing specific atoms and achieving an atom-resolved to shell-resolved structural analysis. By assigning the global optimized configuration to M_0 , ζ can serve as a randomness parameter of the Shannon entropy presenting from the most random shape ($-\ln \zeta \rightarrow \infty$ for $\zeta \rightarrow 0$) to the shape identical to the global structure with minimal energy ($-\ln \zeta = 0$ for $\zeta = 1$). Then, the probability of shape similarity ($P(\zeta)$) can be sampled from the MD trajectory. To construct a 3D diagram representing the change in $P(\zeta)$ along the temperature axis, an NVT MD simulation was performed at 10 K increments. This MD simulation predicted the canonical ensemble as effectively as a Monte Carlo simulation did [17], and each MD simulation started from the global minimal structure optimized by our previous parallel-tempering-multicanonical-basin-hopping plus genetic-algorithm method [18]. Nevertheless, the rate at which the $P(\zeta)$ decayed increased considerably as the temperature increased. In the 3D diagram, the probability becomes less visible at higher temperatures (Fig. 1, top row). To overcome this visualization problem, the amplitude of the probability was enhanced according to the following temperature-dependent relation:

$$P_{ep}(\zeta, T) = P_{org}(\zeta, T) \times F(T) \quad (0.2)$$

Using this formula, the original probability ($P_{org}(\zeta)$) was transformed to an enhanced probability ($P_{ep}(\zeta)$) by using an F function (Fig. 1, middle row), which is defined as follows:

$$F(T) = \frac{\zeta_{upper}(T) - \zeta_{lower}(T)}{\Delta \zeta_{org} R_{ep}} \quad (0.3)$$

where ζ_{upper} (ζ_{lower}) are the upper (lower) ζ of nonzero $P_{org}(\zeta)$; $\Delta \zeta_{org} = 10^{-4}$ is the original sampling interval along ζ axis; and $[\zeta_{upper} - \zeta_{lower}]/R_{ep}$ ($R_{ep} = 100$) is the new sampling interval in the range of $[\zeta_{lower}, \zeta_{upper}]$. Consequently, the function elevates all of the probabilities along the temperature axis to a comparable level without altering the locations of the probability distributions, resulting in a more reliable contrast in the 2D projection of the probability contour (Fig. 1, bottom row). Interestingly, the tendency of the F function can coincide with that of the Lindemann index [19, 20] (Fig. 2). Because the Lindemann index is a structure-dependent function, this coincidence showed that the bond length fluctuation (δ , see Appendix) can be reflected by the similarity bandwidth ($\zeta_{upper} - \zeta_{lower}$), which is related to the standard deviation of the probability distribution of shape similarity.

The advantage of this method is that shape similarity can be specified by the substructure of a cluster. For example, the F function of the $Ag_{17}Cu_2$ substructure, excluding the atoms along the C_5 rotational axis, precisely predicted a sudden and significant increase in the Lindemann index at approximately 500 K (Fig. 3(b) and 3(c)). However, the entire $Ag_{17}Cu_2$ cluster lacks such characteristics (Fig. 6(a)), reflecting that the C_5 atoms contribute the most to the Lindemann index. The same conclusion can be reached by comparing the F functions of the whole atoms (Fig. 6(a)) with those of the outer surface atoms (Fig. 3(c)) of $Cu_{13}Ag_1$. The two-step process of the outer surface atoms at less than 600 K shows that the change of the Lindemann index (Fig. 3(b)) was influenced by the movement of the central (Ag) atom. This is because in clusters, any movement of an atom will closely affect the position of the surrounding atoms. Therefore, certain atoms can be traced by excluding them from shape similarity calculations (i.e., targeting only the surrounding atoms). This substructure approach involves implementing atomic labeling for both $M_{0,j}$ and $M_j(t)$ after the MD trajectory is complete. In this study, demonstrations of shape similarity analysis were provided, including the $P(\zeta)$ s of entire clusters and those excluding the central (C_5) atoms of $n = 14$ ($Ag_{17}Cu_2$) clusters. Large clusters, such as $Ag_{32}Cu_6$ and $Ag_{32}Cu_{13}$, were divided into core and shell substructures.

Results

Introducing shape similarity analysis revealed the physical meaning of ζ and that of the bandwidth of $P(\zeta)$ distribution, the F function. However, the most intriguing result is the effect of temperature on distribution variation. To obtain a globally appearing $P(\zeta)$, the 3D $P_{ep}(\zeta, T)$ was projected onto a $\zeta - T$ plane to display the enhanced probability contours (EPC); the amplitude of the probability is marked in the color bar (Fig. 3(d), 3(e), 4, 5(c), and 5(d)). These shape distributions have three basic features:

1. Multiple distributions can exist within a certain temperature range.
2. Certain distributions smoothly transition into one to another, whereas some are separated by a basin or a broken ridge.
3. The major peak of $P(\zeta)$ lies within a certain bandwidth of ζ . The bandwidth shifts from higher $\zeta (\approx 1)$ to lower $\zeta (\rightarrow 0)$ while T is increasing.

In cluster melting, instead of abruptly changing as in bulk systems, the width of the peak broadens in specific heat. This broadening has been widely discussed from the perspectives of energy [12, 21–23], vibration spectrum [24] (e.g., velocity autocorrelation function or instantaneous normal mode), and structural order parameters [5, 25] (e.g., atomic bond length fluctuation or common neighbor analysis). These findings indicate that shape differentiates clusters from bulk systems. According to the maximal entropy study by Poland [26], the peak of specific heat is broadened when more energy states coexist, which implies the coexistence of complex phases. In the EPC diagrams, the phase transition of clusters is clearly driven by the probable coexistence of distinct shapes.

Let us first examine the EPCs of $Ag_{13}Cu_1$ and $Ag_{17}Cu_2$, of which $P(\zeta)$ s have a monotonic displacement from the higher bandwidth (0.8,1) to the middle bandwidth (0.2,0.8) as the temperature increases (Figs. 3(d) and 4(a)). The major transition (displacement) of the bandwidth predicts the melting points of the specific heat approximately 1,000 K for $Ag_{13}Cu_1$ and 900 K for $Ag_{17}Cu_2$ —they just behave similarly to the classical solid-liquid transition. Nevertheless, there have been prominent discussions regarding the mystery *prepeak* of specific heat, which usually lies between the solid phase and the melting point. Regarding shape, one can avoid ambiguous solid/liquid descriptions for finite-size clusters. The representative case of the prepeak is $Cu_{13}Ag_1$ cluster (Figs. 3(a)). Starting from T = 0, it maintains Brownian motion from its ground state structure ($1 > \zeta > 0.9$) (Fig. 4(c)). At a still lower temperature (300 K), the probabilities suddenly spread toward lower ζ (approximately 0.6), which contributes to the existence of the prepeak of the specific heat. Because the shape database of the trajectory has been constructed in the process of shape recognition, the parameter (ζ, T) can be used to easily retrieve the configurations corresponding to the peaks of these probabilities from the database, elucidating atomic behavior (Fig. 7–10). For instance, from the representative configurations of the $Cu_{13}Ag_1$ cluster, it appears that the spreading distribution was caused by the movement of the central atom and adatom (Fig. 7(a), T = 680 K). To know precisely how the central atom influences the structural changes, the EPC of the substructure can be examined excluding the central atom; these are referred to as the outer atoms (Fig. 3(c) and 4(d)). At approximately 320 K, the EPC spread a narrower distribution to the lower ζ (approximately 0.7), at which the central atom still occupied its original position, but the adatom started to move around on the surface (Fig. 7(b)). Then, at approximately 570 K to 680 K, a notable shift of distribution to a lower bandwidth of ζ (0.4,0.7) indicated that the original central atom was replaced by another atom (Fig. 7(b)), indicating that the Lindemann index and F function of the outer atoms demonstrated a similar two-step behavior (Fig. 3(b) and 3(c)). The central Cu atom of $Ag_{13}Cu_1$, however, never escaped from its surrounding atoms (Fig. 4(a) and 8(a)). Therefore, the outer surface atoms of $Ag_{13}Cu_1$ are more stable compared to those of $Cu_{13}Ag_1$ until 800 K, the temperature at which the shapes without any adatom contribute a separated distribution value of approximately 0.65 for the ζ (Fig. 4(b) and Fig. 8(b)). Although these observations were supplemented by pure statistics derived from the shape information, the EPC can recover the structural evolution of cluster melting without tedious dynamical analysis of the trajectory. By using the substructure approach, shape similarity becomes more sensitive to any atomic movement. A case study of the $Ag_{17}Cu_2$ substructure, excluding the atoms along the C_5 rotational axis, revealed that a detailed atom relocation could be captured if the substructure is designed wisely (Fig. 3(e) and 9(b)). A considerable change in the EPC as well as in the Lindemann index at approximately 500 K shows that the linear orientation of the C_5 atom bends, whereas the shape similarity of the entire $Ag_{17}Cu_2$ cluster does not represent such phenomenon. (Fig. 3(d) and 9(a)). Incorporating shape similarity with the substructure facilitates tracing the behavior of any amount of atoms, and does not require that iterated visual inspections be involved in the trajectory. The probability distributions not only coexist but also generally cover a wide range of temperature (e.g., some probabilities of $\zeta \approx 0.8$ still remain until 2,000 K for the $Cu_{13}Ag_1$ cluster). Moreover, starting from 1,500 K for Ag-rich clusters and 2,200 K for Cu-rich clusters, a distinct distribution of extreme lower similarities ($0.3 > \zeta > 0$) was discovered coexisting with the medium distributions ($0.6 > \zeta > 0.3$) (Fig. 3(d), 3(e), and 4). Such distributions at high temperatures should be universal during the dissociation transition [27–30].

Finally, using core/shell substructures is proposed; these substructures are suitable for analyzing large quantities

of material to demonstrate the potential applications of shape similarity. Because Ag-Cu nanoclusters are widely used in research [31–39], the implementation of a core/shell substructure will considerably simplify the structural analysis in trajectory or in Monte Carlo sampling. This general idea can be effectively delivered by analyzing $Ag_{32}Cu_6$ cluster, of which the core (Cu) atoms form a hexagonal planar structure (Fig. 10(a)); $Ag_{32}Cu_{13}$ cluster could also be analyzed because its Cu atoms form an icosahedral core structure (Fig. 10(b)). Regarding the $Ag_{32}Cu_6$ cluster, an abrupt change (disconnection of the distributions) occurs in the EPCs of its core substructures at approximately 500–600 K, which contributes to the first sharp peak in the specific heat (Fig. 5(a) and 5(c)). The representative configurations of $P(\zeta)$ confirmed that the planar structure of the Cu atoms of $Ag_{32}Cu_6$ transformed into two types of 3D core structures (Fig. 10(a), $\zeta \approx 0.67$ and $\zeta \approx 0.61$ at 700 K). In addition, the icosahedral core atoms of $Ag_{32}Cu_{13}$ become irregularly shaped (approximately 500 K), exhibiting decreased bandwidth ($0.6 > \zeta > 0.3$) (Fig. 5(d) and 10(b), $\zeta \approx 0.41$). A comparable profile was observed between the Lindemann indices and F functions of the core atoms of $Ag_{32}Cu_6$ and $Ag_{32}Cu_{13}$ (Fig. 5(b) and 6(b)). The probability amplitude of $Ag_{32}Cu_{13}$ was suddenly enhanced at approximately 300–400 K, indicating that the shell part was already distorted (Fig. 10(b), $\zeta \approx 0.92$). This phenomenon can be precisely presented by using the EPC of the shell atoms or other substructures. When the core atoms collapse or deform, the entire cluster becomes extremely unstable. Inspecting the EPCs indicated that both clusters experience the melting process at a wide temperature range (e.g., 500–800 K). Again, the terminology *solid* and *liquid* can be avoided, using multiple coexisting distributions of shapes, instead. The coexisting distributions revealed by the EPCs of all of the substructures terminate at 800 K, which corresponds to the main (second) peak of specific heat, demonstrating that only one distribution of shapes (Fig. 10, 900 K) with the medium bandwidth is left after the “melting point”.

Although statistical analysis is applied to shape similarity, the MD simulation facilitates investigating the dynamical properties of clusters. Thus, the self-diffusion coefficient of the i th atom was calculated by integrating the velocity autocorrelation function, as follows:

$$D_i = \frac{1}{3} \int \langle v_i(0) \cdot v_i(t) \rangle dt \quad (0.4)$$

The averaged D values of the core and whole atoms were compared with the averaged shape similarity (Fig. 11). When a molecular system transitions from the solid to liquid phase, its oscillatory motion is gradually weakened by diffusive motion, increasing the diffusion coefficient. By contrast, the EPC captures the diffusive motion by broadening the probability distribution; although this is not straightforward, the probability variations can be interpreted using the enhanced F function. Instead of using the F function, it is also convenient to use $1 - \langle \zeta \rangle_t$ to demonstrate how the cluster structures deviate from the reference configuration. To illustrate the difference between the diffusion coefficient and the similarity deviation, both D and $1 - \langle \zeta \rangle_t$ were plotted as the functions of temperature for the core/whole atoms of $Ag_{32}Cu_6$ and $Ag_{32}Cu_{13}$.

Regarding the diffusion coefficients of $Ag_{32}Cu_6$, both the core and whole atoms increase at approximately 600 K, indicating the initiation of diffusive motion (Fig. 11(a)). In the $1 - \langle \zeta \rangle_t$ diagram, both the core and whole atoms exhibit one-step transition at approximately 500 K. Beyond 600 K, the $1 - \langle \zeta \rangle_t$ of the core atoms gradually increase, whereas that of the whole atoms remain stable until 800 K, then begin to rise again (Fig. 11(b)). According to the EPC, two distributions of 3D core structures compete at 500–800 K (Fig. 5(c)). At beyond 800 K, the probabilities that exhibited high levels of shape similarity ($\zeta \approx 0.67$) survived. The diffusion coefficients of the core/whole atoms of $Ag_{32}Cu_{13}$ demonstrated similar trends compared with those of $Ag_{32}Cu_6$, both increasing at approximately 600 K (Fig. 11(c)). In contrast, the $1 - \langle \zeta \rangle_t$ s of $Ag_{32}Cu_{13}$ present a one-step profile at 400 K and oscillate until 800 K (Fig. 11(d)); after surpassing this temperature, they continue to increase smoothly. Although the difference between $Ag_{32}Cu_6$ and $Ag_{32}Cu_{13}$ is notable regarding shape similarity, it is difficult to distinguish regarding the diffusion coefficient. The EPC shows that the core atoms of $Ag_{32}Cu_{13}$ form three coexisting phases, namely, the crystalline ($\zeta \approx 0.9$), amorphous ($\zeta \approx 0.4$), and medium phases (in-between the highest and the lowest similarity distribution; $\zeta \approx 0.5$; Fig. 5(d)). Three competing phases remained until 800 K, after which only the amorphous phase survived. Moreover, the shape deviation of the core atoms was much higher than was that of the whole atoms (Fig. 11(d)), suggesting that considerable structural changes occurred in the core atoms.

It is clear that ζ is sensitive to the local atomic distribution and captures any atom relocation. Two interchanged atoms may drastically influence both the F function and EPC; the corresponding structural information can be easily retrieved from the shape database. By contrast, the diffusion coefficient lacks a geometrical perspective. To investigate the behaviors of the clusters, the power spectrum density based on the Fourier transformation of the velocity autocorrelation function [24] could be performed and compared to the experimental infrared spectrum. Nevertheless, a trajectory analysis is required to determine the global aspect of the structures [40].

Unlike the diffusion coefficient or power spectrum density, the shape similarity may not directly correlate to the experimental measurements; however, it is possible to associate determining the molecular shapes in the ion

mobility spectrometry [41–44]. In this experiment, the ion or metal clusters were injected into a drift tube by using an electric field, and heated because of collisions with the buffer gas inside the tube. The isomers that formed because of the transient heating were determined based on the distribution of the collision cross-section. It is believed that this cross-section is strongly related to the shape of the isomers and several theoretical approaches have been proposed for calculating the cross-section based on MD simulation [45–50]. Similar to the numerical isothermal Brownian-type MD simulation used in this work, the thermal energy provided to the clusters can be controlled based on the temperature of the drift tube [43]. Nevertheless, in this simulation the presence of a buffer gas was mimicked using the pseudofriction terms in the equations of motion [40]. A model system for charged cluster is also required [?, 51, 52]. Consequently, the isomerization process could be analyzed as a function of temperature, yielding a contour plot of the cross-section or other order parameter distributions versus temperature [49].

Finding a direct relation between the shape similarity and collision cross-section is difficult. Calvo et al. conducted a statistical analysis of the cross-section distribution applied in peptide dynamics [49, 50], concluding that three order parameters were highly correlated to the collision cross-section: the radii of gyration, surface area, and volume of the convex hull. These parameters can be combined to mimic the function of the collision cross-section. The shape similarity provides two contributions to these works:

1. It can serve as an additional order parameter, mimicking the variations of the collision cross-section.
2. It can be used to systematically generate the shape database, filtering out or classifying the shapes of isomers based on statistics.

Using known isomers as the reference configurations is straightforward, enabling multiple EPCs and F functions to be generated; each similarity function corresponds to only one reference configuration. Regarding the numbers of reference configurations, it is suggested that the similarity functions be statistically analyzed. The shape similarity technique has also been applied to a large system, namely, the folding of a transthyretin peptide. Twelve similarity functions were generated for substructures, which were characterized based on residues, and a cross-correlation analysis was performed to evaluate folding dynamics.

Conclusion

Using shape similarity to elucidate phase transitions and cluster melting is a simple and flexible approach that has multiple applications. Its computational cost is low, requiring only a few hours to calculate 250 temperature points (10–2500 K), each of which contains 10^8 molecular snapshots. The accuracy of the transition temperature should strongly depend on the configuration sampling method and model system being studied. In this study, an isothermal Brownian-type MD simulation was performed to simulate cluster heating. The proposed algorithm is reliable and efficient in generating NVT ensembles [17], and is adequate for simulating heating experiments (see the Appendix); however, producing accurate equilibrium properties requires an excessive amount of time to ensure the ergodicity of the system, which has been difficult to achieve using conventional Monte Carlo and MD simulations [53, 54]. To overcome this ergodicity problem, improved algorithms, such as parallel tempering Monte Carlo or replica-exchange MD simulations, should be considered [55–58]. By contrast, the shape recognition technique is advantageous because it can work with any configuration sampling method, depicting how the shape of the cluster evolves throughout the thermal process without inquiring regarding the detailed interactions between atoms. Using EPCs associated with the substructure approach and the efficient configuration restoration from the shape database facilitates intuitively interpreting the phase transition, considering the coexistence and transitions of the shape distributions.. The retrieved configuration corresponding to the peak of the probability distribution statistically reconstructs the behaviors of the substructure. For hundreds or even thousands of atoms, the substructure can be designed in many sophisticated ways to ease the complexity of the analysis. This study demonstrates that core/shell substructures can be systematically assigned (e.g., $Ag_{32}Cu_6$ and $Ag_{32}Cu_{13}$) to extract the symmetrical inner part as the core substructure (e.g., excluding C_5 atoms of $Ag_{17}Cu_2$), or to exclude one atom to achieve the atom-resolved analysis (e.g., the outer surface atoms of $Ag_{13}Cu_1$ and $Cu_{13}Ag_1$). Ultimately, shape similarity is applicable not only for finite-size clusters but also for any type of molecule that presents shape. The dynamical analysis of the folding and unfolding of the peptide molecule was conducted using the same technique. The proposed method should become a powerful tool for studying nanostructures and biological systems.

Appendix

Model system

The commonly used empirical Gupta potential [59] was used to model the many-body interactions among atoms. The total energy E_{total} is explicitly determined as follows:

$$\begin{aligned} E_{total} = & \sum_{i=1}^n \frac{1}{2} m_i v_i^2 \\ & + \sum_{i=1}^n \left[\sum_{j(\neq i)=1}^n A_{ij} \exp[-p_{ij}(\frac{r_{ij}}{r_{ij}^{(0)}} - 1)] \right. \\ & \left. - \left\{ \sum_{j(\neq i)=1}^n \xi_{ij}^2 \exp[-q_{ij}(\frac{r_{ij}}{r_{ij}^{(0)}} - 1)] \right\}^{1/2} \right] \end{aligned} \quad (0.5)$$

where i and j are the atomic indices, and m_i and v_i are the mass and velocity of i th particle, respectively. Regarding the Ag-Cu clusters, three sets of atomic interaction parameters are required (i.e., Ag-Ag, Cu-Cu, and Ag-Cu). Table 1 lists the parameters for each set of values that were obtained by fitting to the lattice constant, cohesive energy, and elastic constants of the bulk face-centered-cubic crystalline structure at 0 K [60]. The $r_{ij}^{(0)}$ (in units of Å; Table 1) for Ag-Cu was calculated by averaging the $r_{ij}^{(0)}$'s of Ag-Ag and Cu-Cu. This empirical potential was used in the MD simulations.

Simulation algorithm and thermal properties.

The isothermal Brownian-type MD simulation was used to conduct the numerical heating experiment for the clusters and applied to calculate the specific heat, as follows:

$$C_V = \frac{\langle E_{total}^2 \rangle_t - \langle E_{total} \rangle_t^2}{n(k_B T)^2} \quad (0.6)$$

. The Lindemann index was determined as follows:

$$\delta = \frac{1}{n(n-1)} \sum_{i=1}^n \sum_{j=1}^n \frac{\sqrt{\langle r_{ij}^2 \rangle_t - \langle r_{ij} \rangle_t^2}}{\langle r_{ij} \rangle_t} \quad (0.7)$$

for Ag-Cu metallic clusters of size n. Each MD simulation was performed at a constant temperature for a total of 10^8 time steps, where one time-step equaled 0.001 ps. The so-called Bulgac-Kusnezov dynamics [61], which are a modified version of the Nosé-Hoover thermostat, were applied [62, 63]. This algorithm has the salient feature that it introduces a cubic coupling scheme for the pseudofriction terms. The coupling scheme has been proven to more effectively control the temperatures of free clusters compared with the original Nosé-Hoover scheme, more rapidly exploring the phase space. However, the disadvantage of this algorithm is that its coupling coefficients are strongly correlated with the temperature and cluster size, making it difficult to integrate equations at high temperatures or when using large clusters [64]. To resolve this dilemma, Ju and Bulgac [65] developed the refined cubic coupling scheme used in this study. In their approach, the temperature and cluster size are explicitly incorporated in the pseudofriction coefficients. The quality of this improved scheme has been critically examined, proving that it is applicable to various metallic clusters [17].

References

- [1] Anne K Starace, Baopeng Cao, Oscar H Judd, Indrani Bhattacharyya, and Martin F Jarrold. Melting of size-selected aluminum nanoclusters with 84-128 atoms. *The Journal of chemical physics*, 132(3):034302, 2010.
- [2] Martin Schmidt and Hellmut Haberland. Phase transitions in clusters. *C R Physique*, 3(3):327–340, 2002.
- [3] Francesca Baletto and Riccardo Ferrando. Structural properties of nanoclusters: Energetic, thermodynamic, and kinetic effects. *Reviews of Modern Physics*, 77(1):371–423, 2005.
- [4] Y J Lee, J Y Maeng, E K Lee, B Kim, S Kim, and K K Han. Melting behaviors of icosahedral metal clusters studied by Monte Carlo simulations. *Journal of Computational Chemistry*, 21(5):380–387, 2000.

- [5] Ali Sebetci and Ziya B Guvenc. Molecular Dynamics Simulation of the Melting Behaviours of 12-, 13-, 14-Atom Icosahedral Platinum Clusters. *Modelling and Simulation in Materials Science and Engineering*, 12:1131, 2004.
- [6] Murat Atis, Hüseyin Aktaş, and Ziya B Güvenç. Structures and melting of Ag N (N=7,12-14) clusters. *Modelling and Simulation in Materials Science and Engineering*, 13(8):1411–1432, December 2005.
- [7] E K Yildirim, M Atis, and Z B Güvenc. Molecular dynamics simulation of melting behaviour of small gold clusters: Au N (N=12-14). *Physica Scripta*, 75(1):111–118, January 2007.
- [8] Hong-Hai Liu, En-Yong Jiang, Hai-Li Bai, Ping Wu, Zhi-Qing Li, and Chang Q Sun. Dislocation stimulus dependence of atomic collective vibration in an icosahedral cluster. *Journal of Nanoscience and Nanotechnology*, 9(8):4668–4672, 2009.
- [9] Florent Calvo. Solid-solution precursor to melting in onion-ring Pd-Pt nanoclusters: a case of second-order-like phase change? *Faraday Discussions*, 138:75–88; discussion 119–135, 433–434, 2008.
- [10] Charles Cleveland, W Luedtke, and Uzi Landman. Melting of Gold Clusters: Icosahedral Precursors. *Physical Review Letters*, 81(10):2036–2039, 1998.
- [11] D Schebarchov and S C Hendy. Transition from Icosahedral to Decahedral Structure in a Coexisting Solid-Liquid Nickel Cluster. *Physical Review Letters*, 95(11):7, 2005.
- [12] Z Kuntová, G Rossi, and R Ferrando. Melting of core-shell Ag-Ni and Ag-Co nanoclusters studied via molecular dynamics simulations. *Physical Review B*, 77(20):1–8, 2008.
- [13] Yanting Wang, S Teitel, and Christoph Dellago. Melting and Equilibrium Shape of Icosahedral Gold Nanoparticles. *Chemical Physics Letters*, 394(4-6):4, 2003.
- [14] Jerry O Ebalunode and Weifan Zheng. Molecular shape technologies in drug discovery: methods and applications. *Current Topics in Medicinal Chemistry*, 10(6):669–679, 2010.
- [15] Pedro J Ballester, Isaac Westwood, Nicola Laurieri, Edith Sim, and W Graham Richards. Prospective virtual screening with Ultrafast Shape Recognition: the identification of novel inhibitors of arylamine N-acetyltransferases. *Journal of the Royal Society, Interface / the Royal Society*, 7(43):335–42, February 2010.
- [16] Edward O Cannon, Florian Nigsch, and John B O Mitchell. A novel hybrid ultrafast shape descriptor method for use in virtual screening. *Chemistry Central journal*, 2:3, January 2008.
- [17] S K Lai, W D Lin, K L Wu, W H Li, and K C Lee. Specific heat and Lindemann-like parameter of metallic clusters: mono- and polyvalent metals. *The Journal of chemical physics*, 121(3):1487–98, July 2004.
- [18] P J Hsu and S K Lai. Structures of bimetallic clusters. *The Journal of chemical physics*, 124(4):044711, 2006.
- [19] F. A. Lindemann. The calculation of molecular Eigen-frequencies. *Phys. Z.*, 11:609, 1910.
- [20] Thomas L. Beck, Julius Jellinek, and R. Stephen Berry. Rare gas clusters: Solids, liquids, slush, and magic numbers. *The Journal of Chemical Physics*, 87(1):545, 1987.
- [21] Young Joo Lee, Eok-Kyun Lee, Sehun Kim, and R. Nieminen. Effect of Potential Energy Distribution on the Melting of Clusters. *Physical Review Letters*, 86(6):999–1002, February 2001.
- [22] Gary A Breaux, Colleen M Neal, Baopeng Cao, and Martin F Jarrold. Melting, premelting, and structural transitions in size-selected aluminum clusters with around 55 atoms. *Physical Review Letters*, 94(17):173401, 2005.
- [23] Eva G Noya, Jonathan P K Doye, and Florent Calvo. Melting of aluminium clusters. 2006.
- [24] Ping-Han Tang, Ten-Ming Wu, Tsung-Wen Yen, S K Lai, and P J Hsu. Comparative study of cluster Ag(17)Cu(2) by instantaneous normal mode analysis and by isothermal Brownian-type molecular dynamics simulation. *The Journal of chemical physics*, 135(9):094302, 2011.
- [25] S.K. Lai, Yu-Ting Lin, P.J. Hsu, and S.a. Cheong. Dynamical study of metallic clusters using the statistical method of time series clustering. *Computer Physics Communications*, 182(4):1013–1026, April 2011.

- [26] Douglas Poland. Intermediates in the melting transitions of aluminum nanoclusters. *The Journal of chemical physics*, 126(5):054507, 2007.
- [27] R. Werner. Melting and evaporation transitions in small Al clusters: canonical Monte-Carlo simulations. *The European Physical Journal B*, 43(1):47–52, February 2005.
- [28] M Wanner, R Werner, and D Gerthsen. Dynamics of gold clusters on amorphous carbon films induced by annealing in a transmission electron microscope. *Surface Science*, 600:632–640, 2006.
- [29] M Schmidt, T Hippler, J Donges, W Kronmüller, B Von Issendorff, H Haberland, and P Labastie. Caloric curve across the liquid-to-gas change for sodium clusters. *Physical Review Letters*, 87(20):203402, 2001.
- [30] F Calvo. Kinetic approach to the cluster liquid-gas transition. 2004.
- [31] Daojian Cheng, Xin Liu, Dapeng Cao, Wenchuan Wang, and Shiping Huang. Surface segregation of Ag-Cu-Au trimetallic clusters. *Nanotechnology*, 18(47):475702, 2007.
- [32] Giovanni Barcaro, Alessandro Fortunelli, Giulia Rossi, Florin Nita, and Riccardo Ferrando. Electronic and structural shell closure in AgCu and AuCu nanoclusters. *The journal of physical chemistry. B*, 110(46):23197–23203, 2006.
- [33] Yi Rao, Yimin Lei, Xiangyuan Cui, Zongwen Liu, and Fuyi Chen. Optical and magnetic properties of Cu-doped 13-atom Ag nanoclusters. *Journal of Alloys and Compounds*, 565(0):50–55, 2013.
- [34] G Rossi, A Rapallo, C Mottet, A Fortunelli, F Baletto, and R Ferrando. Magic polyicosahedral core-shell clusters. *Physical Review Letters*, 93(10):105503, 2004.
- [35] F Baletto, C Mottet, and R Ferrando. Time evolution of Ag-Cu and Ag-Pd core-shell nanoclusters. *The European Physical Journal D Atomic Molecular and Optical Physics*, 24(1-3):233–236, 2003.
- [36] Giovanni Barcaro and Alessandro Fortunelli. A study of bimetallic Cu-Ag, Au-Ag and Pd-Ag clusters adsorbed on a double-vacancy-defected MgO(100) terrace. *Faraday discussions*, 138:37–47; discussion 119–135, 433–434, 2008.
- [37] C Mottet, G Rossi, F Baletto, and R Ferrando. Single impurity effect on the melting of nanoclusters. *Physical review letters*, 95(3):035501, 2005.
- [38] Perla B. Balbuena, Julibeth M. Martinez De La Hoz, and Rafael Callejas Tovar. Size effect on the stability of Cu-Ag nanoalloys. *Molecular Simulation*, 35(10-11):785–794, 2009.
- [39] Suk Jun Kim, Eric a. Stach, and Carol a. Handwerker. Fabrication of conductive interconnects by Ag migration in Cu-Ag core-shell nanoparticles. *Applied Physics Letters*, 96(14):144101, 2010.
- [40] P J Hsu, J S Luo, S K Lai, J F Wax, and J-L Bretonnet. Melting scenario in metallic clusters. *The Journal of chemical physics*, 129(19):194302, November 2008.
- [41] Ph. Dugourd, R. R. Hudgins, D. E. Clemmer, and M. F. Jarrold. High-resolution ion mobility measurements. *Review of Scientific Instruments*, 68(2):1122, 1997.
- [42] Alexandre A. Shvartsburg, Robert R. Hudgins, Philippe Dugourd, and Martin F. Jarrold. Structural Elucidation of Fullerene Dimers by High-Resolution Ion Mobility Measurements and Trajectory Calculation Simulations. *The Journal of Physical Chemistry A*, 101(9):1684–1688, February 1997.
- [43] David E Clemmer and Martin F Jarrold. SPECIAL FEATURE : Ion Mobility Measurements and their Applications to Clusters and Biomolecules. *J. Mass Spectrosc.*, 32(April):577–592, 1997.
- [44] A A Shvartsburg and M F Jarrold. Solid clusters above the bulk melting point. *Physical Review Letters*, 85(12):2530–2, 2000.
- [45] M F Mesleh, J M Hunter, A A Shvartsburg, G C Schatz, and M F Jarrold. Structural Information from Ion Mobility Measurements: Effects of the Long-Range Potential. *The Journal of Physical Chemistry*, 100(40):16082–16086, 1996.

- [46] Robert R Hudgins, Mark A Ratner, and Martin F Jarrold. Design of helices that are stable in vacuo. *J. Am. Chem. Soc.*, 120(49):12974–12975, 1998.
- [47] Thomas Wyttenbach, John E Bushnell, and Michael T Bowers. Salt Bridge Structures in the Absence of Solvent? The Case for the Oligoglycines. *J. Am. Chem. Soc.*, 120(20):5098–5103, 1998.
- [48] F A Fernandez-Lima, H Wei, Y Q Gao, and D H Russell. On the structure elucidation using ion mobility spectrometry and molecular dynamics. *The journal of physical chemistry. A*, 113(29):8221–8234, 2009.
- [49] Fabien Chirot, Florent Calvo, Florian Albrieux, Jérôme Lemoine, Yury O. Tsybin, and Philippe Dugourd. Statistical Analysis of Ion Mobility Spectrometry. I. Unbiased and Guided Replica-Exchange Molecular Dynamics. *Journal of The American Society for Mass Spectrometry*, 23(2):386–396, 2012.
- [50] Florent Calvo, Fabien Chirot, Florian Albrieux, Jérôme Lemoine, Yury O. Tsybin, Pascal Pernot, and Philippe Dugourd. Statistical Analysis of Ion Mobility Spectrometry. II. Adaptively Biased Methods and Shape Correlations. *Journal of The American Society for Mass Spectrometry*, 23(7):1279–1288, 2012.
- [51] F. Calvo. Phenomenological model for the statistical study of charged metal clusters. *Physical Review B*, 60(23):15601–15604, December 1999.
- [52] F Calvo and F Spiegelmann. Mechanisms of phase transitions in sodium clusters: From molecular to bulk behavior. *The Journal of Chemical Physics*, 112(6):2888–2908, 2000.
- [53] J. P. Neirotti, F. Calvo, David L. Freeman, and J. D. Doll. Phase changes in 38-atom Lennard-Jones clusters. I. A parallel tempering study in the canonical ensemble. *The Journal of Chemical Physics*, 112(23):10340, 2000.
- [54] F. Calvo, J. P. Neirotti, David L. Freeman, and J. D. Doll. Phase changes in 38-atom Lennard-Jones clusters. II. A parallel tempering study of equilibrium and dynamic properties in the molecular dynamics and microcanonical ensembles. *The Journal of Chemical Physics*, 112(23):10350, 2000.
- [55] E. Marinari and G. Parisi. Simulated Tempering - A New Monte-carlo Scheme. *Europhysics Letters*, 19(6):451–458, 1992.
- [56] Robert H. Swendsen and Jian-Sheng Wang. Replica Monte Carlo Simulation of Spin-Glasses. *Physical Review Letters*, 57(21):2607–2609, 1986.
- [57] Yuji Sugita and Yuko Okamoto. Replica-exchange molecular dynamics method for protein folding. *Chemical Physics Letters*, 314(November):141–151, 1999.
- [58] Manuel Athènes and Florent Calvo. Multiple-replica exchange with information retrieval. *Chemphyschem : a European journal of chemical physics and physical chemistry*, 9(16):2332–2339, 2008.
- [59] Raju Gupta. Lattice relaxation at a metal surface. *Physical Review B*, 23(12):6265–6270, 1981.
- [60] C. Mottet, G. Tréglia, and B. Legrand. Structures of a Ag monolayer deposited on Cu (111), Cu (100), and Cu (110) substrates: An extended tight-binding quenched-molecular-dynamics study. *Physical Review B*, 46(24):16018, 1992.
- [61] A Bulgac and D Kusnezov. Canonical ensemble averages from pseudomicrocanonical dynamics. *Physical Review A*, 42(8):5045–5048, 1990.
- [62] Shuichi Nosé. A molecular dynamics method for simulations in the canonical ensemble. *Molecular Physics*, 52(2):255–268, 1984.
- [63] William G Hoover. Canonical dynamics: Equilibrium phase-space distributions. *Physical Review A*, 31(3):1695–1697, 1985.
- [64] Aurel Bulgac and Dimitri Kusnezov. Thermal properties of Na₈ microclusters. *Physical review letters*, 68(9):1335–1338, 1992.
- [65] Nengjiu Ju and Bulgac Aurel. Finite-temperature properties of sodium clusters. *Physical Review B*, 48(4):2721, 1993.

Figure 1: The original probability contours (top row, (a) and (d)), the corresponding F functions (middle row, (b) and (e)), and the enhanced probability contours (bottom row, (c) and (f)) of the whole atoms of $Ag_{32}Cu_6$ (left column, (a), (b), and (c)) and $Ag_{32}Cu_{13}$ (right column, (d), (e), and (f)). The image contrast of the probability contour was strongly enhanced, particularly in the high temperature region. The waviness at values surpassing 1100 K occurred because of fluctuations of the upper and lower boundaries of the shape similarity indices at $\zeta_{upper}(T)$ and $\zeta_{lower}(T)$, respectively, whose values were assumed to have a nonzero probability.

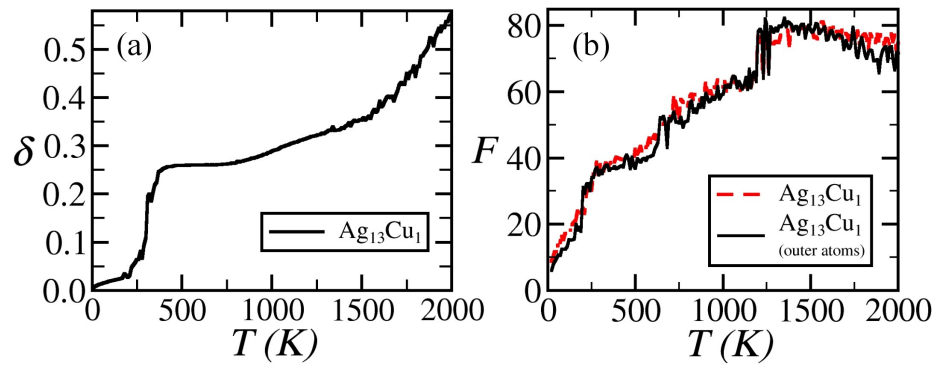


Figure 2: (a) The Lindemann index of $Ag_{13}Cu_1$ demonstrated a similar profile as (b) the F functions corresponding to the EPCs of whole $Ag_{13}Cu_1$ atoms (red dashed) and the outer surface atoms of $Ag_{13}Cu_1$ (black solid).

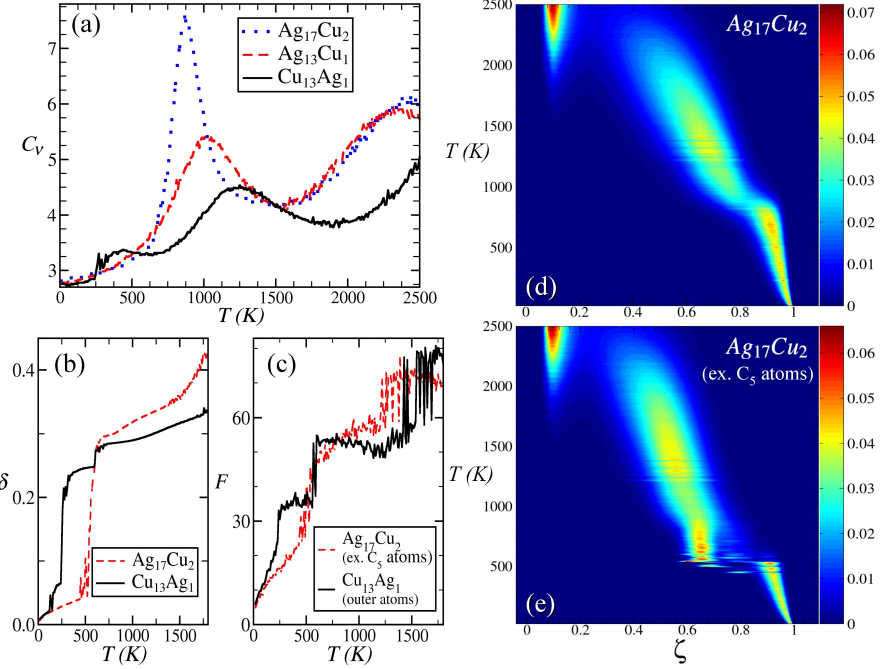


Figure 3: (Color online) (a) The specific heats of $\text{Ag}_{17}\text{Cu}_2$ (blue dotted), $\text{Ag}_{13}\text{Cu}_1$ (red dashed), and $\text{Cu}_{13}\text{Ag}_1$ (black solid); (b) the Lindemann indices of $\text{Ag}_{17}\text{Cu}_2$ (red dashed) and $\text{Cu}_{13}\text{Ag}_1$ (black solid); (c) the F functions versus temperature corresponding to the EPCs of $\text{Ag}_{17}\text{Cu}_2$ without atoms along the C_5 rotational axis (red dashed) and outer surface atoms of $\text{Cu}_{13}\text{Ag}_1$ (black solid); and the EPCs of (d) whole $\text{Ag}_{17}\text{Cu}_2$ atoms and (e) the outer surface atoms (outside the C_5 rotational axis) of $\text{Ag}_{17}\text{Cu}_2$. The color platelet measures the amplitude of $P_{ep}(\zeta, T)$.

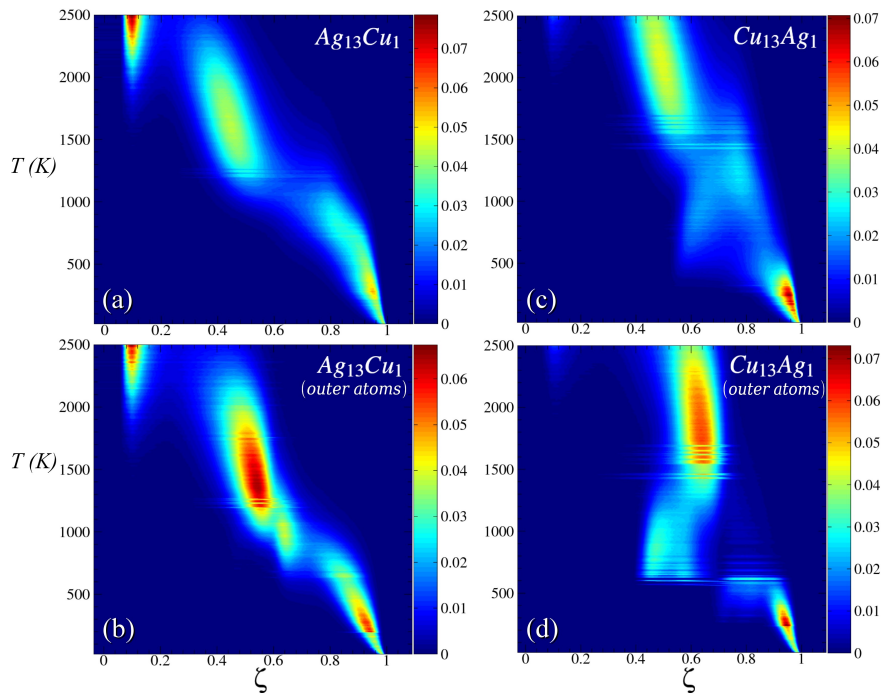


Figure 4: (Color online) The EPCs of (a) whole $Ag_{13}Cu_1$ atoms, (b) the outer surface atoms of $Ag_{13}Cu_1$, (c) whole $Cu_{13}Ag_1$ atoms, and (d) the outer surface atoms of $Cu_{13}Ag_1$. The color platelet measures the amplitude of $P_{ep}(\zeta, T)$.

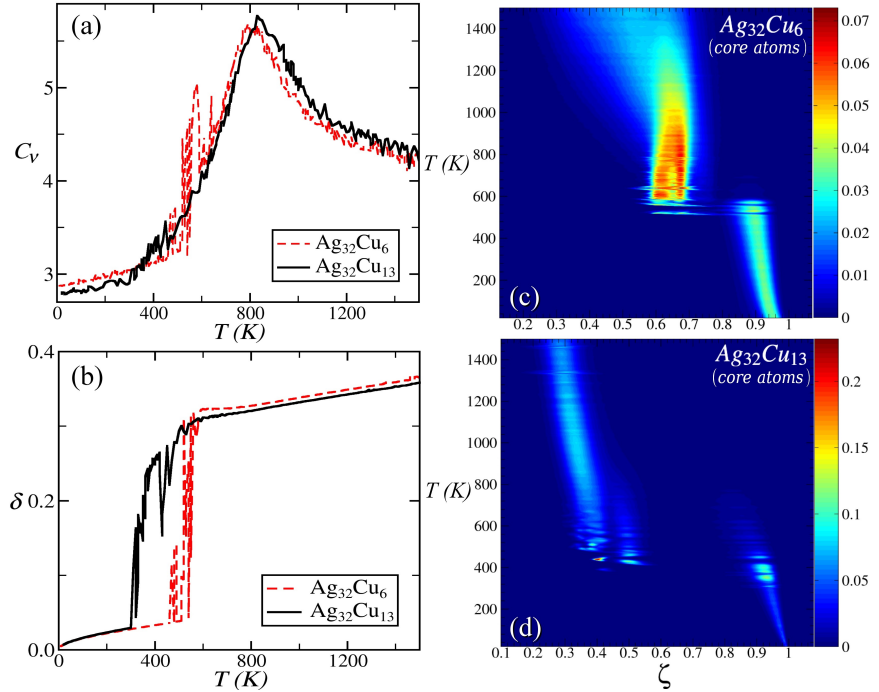


Figure 5: (Color online) (a) The specific heats of $Ag_{32}Cu_6$ (red dashed) and $Ag_{32}Cu_{13}$ (black solid); (b) the Lindemann indices of $Ag_{32}Cu_6$ (red dashed) and $Ag_{32}Cu_{13}$ (black solid); and the EPCs of the core (Cu) atoms of the (c) $Ag_{32}Cu_6$ and (d) $Ag_{32}Cu_{13}$ clusters. The color platelet is used to measure the amplitude of $P_{ep}(\zeta, T)$.

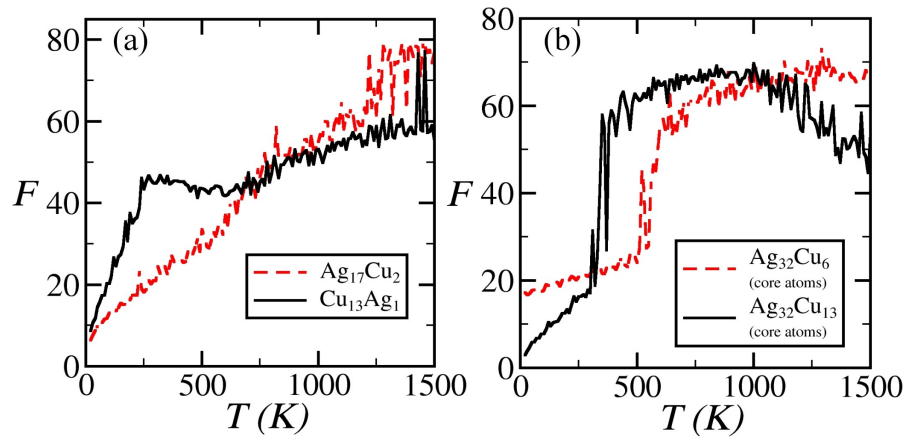
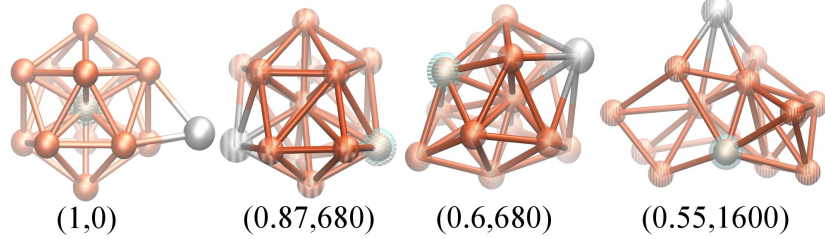


Figure 6: The F functions corresponding to the EPCs of (a) whole $\text{Ag}_{17}\text{Cu}_2$ atoms (red dashed), (a) whole $\text{Cu}_{13}\text{Ag}_1$ atoms (black solid), (b) the core (Cu) atoms of $\text{Ag}_{32}\text{Cu}_6$ (red dashed), and (b) the core (Cu) atoms of $\text{Ag}_{32}\text{Cu}_{13}$ (black solid).

(a) $Cu_{13}Ag_1$



(b) $Cu_{13}Ag_1$ (outer atoms)

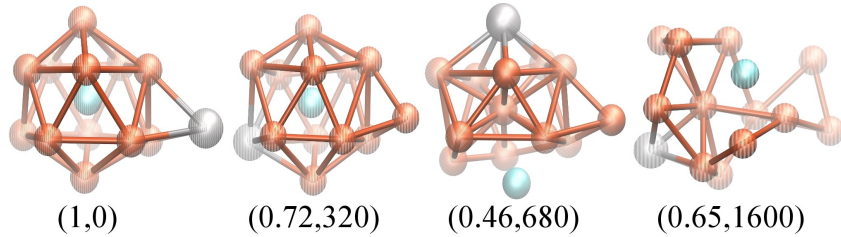


Figure 7: (Color online) The configurations of (a) whole $Cu_{13}Ag_1$ atoms and (b) the outer surface atoms of $Cu_{13}Ag_1$ were obtained from the shape similarity database by using the parameter (ζ, T) . The global structure corresponds to $\zeta = 1$ and $T = 0$ K (1,0). The red atom refers to Cu and the silver atom indicates Ag. The imperceptible atom of the substructure in (b) is drawn as unbonded. The original central atom is labeled in cyan to demonstrate its new position when the structure changes.

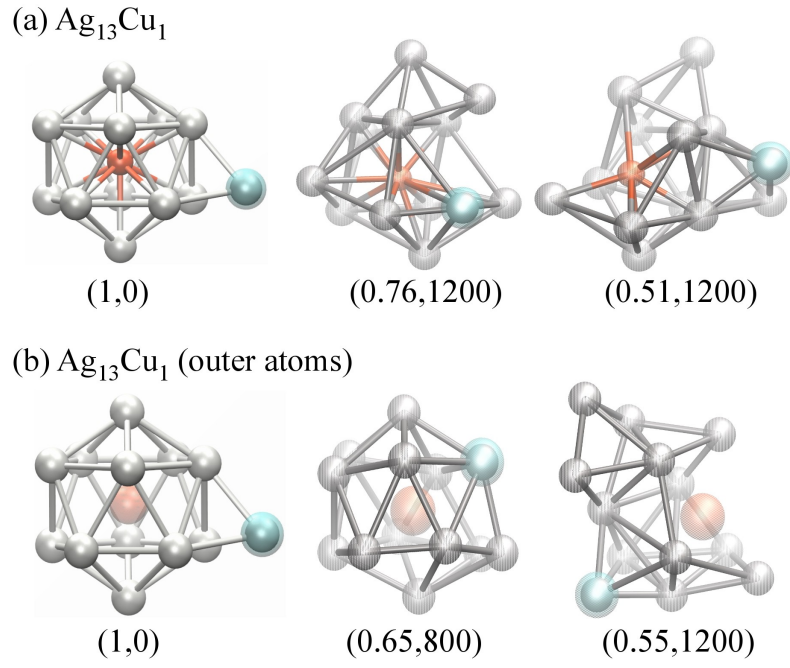
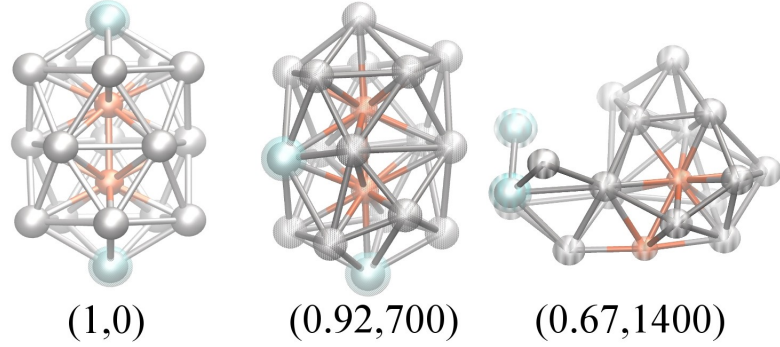


Figure 8: (Color online) The configurations of (a) whole $Ag_{13}Cu_1$ atoms and (b) the outer surface atoms of $Ag_{13}Cu_1$ were obtained from the shape similarity database by using the parameter (ζ, T) . The global structure corresponds to $\zeta = 1$ and $T = 0$ K (1,0). The red atom refers to Cu and the silver atom indicates Ag. The imperceptible atom of the substructure in (b) is drawn as unbonded. The original adatom is labeled in cyan to demonstrate its new position when the structure changes.

(a) $Ag_{17}Cu_2$



(b) $Ag_{17}Cu_2$ (ex. C_5 atoms)

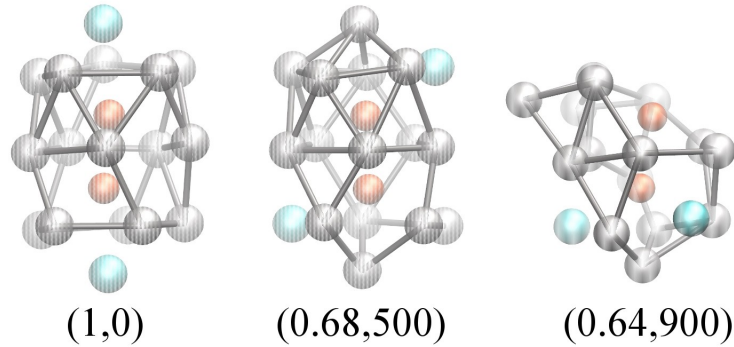
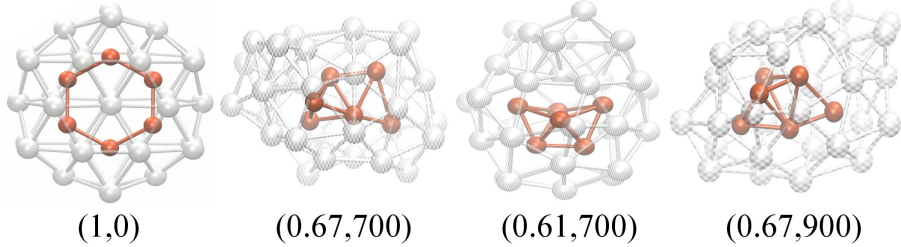


Figure 9: (Color online) The configurations of (a) whole $Ag_{17}Cu_2$ atoms and (b) $Ag_{17}Cu_2$ excluding atoms along the C_5 rotational axis were obtained from the shape similarity database by using the parameter (ζ, T) . The global structure corresponds to $\zeta = 1$ and $T = 0$ K (1,0). The red atom refers to Cu and the silver atom indicates Ag. The imperceptible C_5 atoms of the substructure in (b) are drawn as unbonded. The original top and bottom C_5 atoms of $Ag_{17}Cu_2$ are labeled in cyan to demonstrate their new positions when the structure changes.

(a) $Ag_{32}Cu_6$ (core atoms)



(b) $Ag_{32}Cu_{13}$ (core atoms)

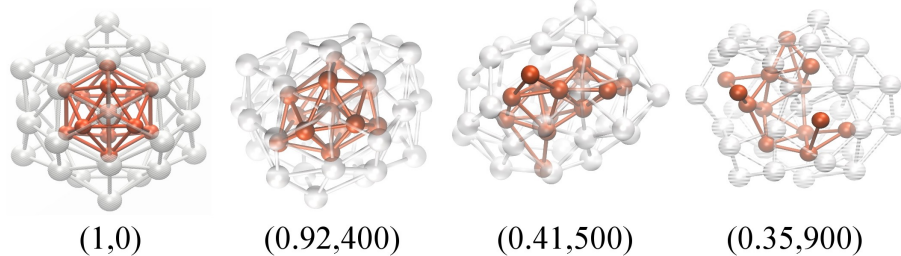


Figure 10: (Color online) The configurations of (a) the core (Cu/red) atoms of $Ag_{32}Cu_6$, and (b) the core (Cu/red) atoms of $Ag_{32}Cu_{13}$ were obtained from the shape similarity database by using the parameter (ζ, T) . The global structure corresponds to $\zeta = 1$ and $T = 0$ K (1,0). The shell (Ag) atoms are presented in silver to enable the shell configurations to be simultaneously analyzed.

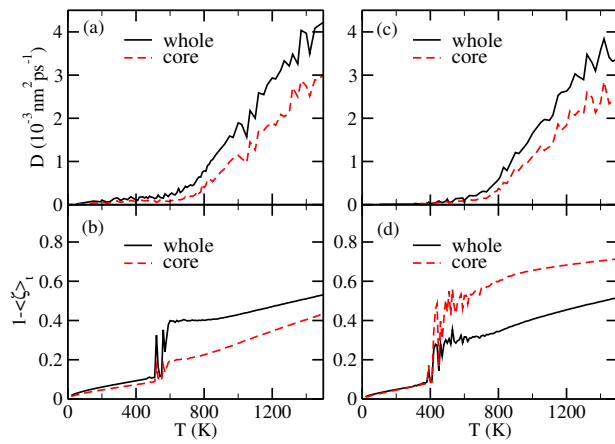


Figure 11: (Color online) The averaged self-diffusion coefficient D (top row) and the $1 - \langle \zeta \rangle_t$ function (bottom row) versus temperature of the core (red dashed) and whole atoms (black solid) of $\text{Ag}_{32}\text{Cu}_6$ ((a) and (b)) and $\text{Ag}_{32}\text{Cu}_{13}$ ((c) and (d)).

Table 1: Gupta potential parameters for the bimetallic cluster Ag-Cu.

ij	A_{ij} (eV)	ξ_{ij}	p_{ij}	q_{ij}	$r_{ij}^{(0)}$
Cu-Cu	0.0894	1.2799	10.550	2.430	2.560
Ag-Cu	0.0977	1.2275	10.700	2.805	2.725
Ag-Ag	0.1031	1.1895	10.850	3.180	2.890